Charge-Lattice Coupling in Hole-Doped LuFe_{2}O_{4+δ}: The Origin of Second-Order Modulation

Shiqing Deng, Lijun Wu, Hao Cheng, Jin-Cheng Zheng, Shaobo Cheng, Jun Li, Wenbin Wang, Jian Shen, Jing Tao, Jing Zhu, and Yimei Zhu

Phys. Rev. Lett. **122**, 126401 — Published 27 March 2019

DOI: 10.1103/PhysRevLett.122.126401

Charge-lattice coupling in hole-doped $LuFe_2O_{4+\delta}$: the origin of second order modulation

Shiqing Deng,[1,2,^] Lijun Wu,[2] Hao Cheng,[3] Jin-Cheng Zheng,[3] Shaobo Cheng,[1,2] Jun Li,[2] Wenbin Wang,[4] Jian Shen,[5] Jing Tao,[2] Jing Zhu,[1,†] and Yimei Zhu[2,*]

[1]*School of Materials Science and Engineering, Tsinghua University, Beijing 100084, P. R. China;*

[2]*Condensed Matter Physics and Materials Science Department, Brookhaven National Laboratory, Upton, NY 11973, USA;*

[3]*Department of Physics, Xiamen University, Xiamen 361005, P. R. China;*

[4]*Institute of Nanoelectronic Devices and Quantum Computing, Fudan University, Shanghai 200433, P. R. China;*

[5]*Department of Physics, Fudan University, Shanghai 200433, P. R. China.*

Abstract

Understanding singularities in ordered structures, such as dislocations in lattice modulation and solitons in charge ordering, offers great opportunities to disentangle the interactions between the electronic degrees of freedom and the lattice. Specifically, a modulated structure has traditionally been expressed in the form of discrete Fourier series with *constant* phase and amplitude for each component. Here, we report atomic scale observation and analysis of a new modulation wave in hole-doped $LuFe_2O_{4+\delta}$ that requires significant modifications to the conventional modeling of ordered structures. This new modulation with an unusual *quasiperiodic* singularity can be accurately described only by introducing a well-defined secondary modulation-vector in both the phase and amplitude parameter spaces. Correlated with density-functional-theory calculations our results reveal that those singularities originate from the discontinuity of lattice displacement induced by interstitial oxygen in the system. The approach of our work is applicable to a wide range of ordered systems, advancing our understanding of the nature of singularity and modulation.

Keywords: second order incommensurate modulation, charge ordering, quasi-periodic lattice

displacement, singularity, lutetium ferrite.

Main text

Symmetry-breaking in quantum states is one of the central topics in modern condensed matter physics and is widely considered to be the driving force of the emergent properties such as high-temperature superconductivity (HTSC), colossal magnetoresistance (CMR) and topological behavior [1-6]. Often the symmetry-breaking in quantum states results in electronic and lattice modulation, for example, charge and/or spin density wave [7,8], charge order (CO) [9] and periodic lattice displacement (PLD) [10]. It is well-known that the characterization of those modulations plays a key role in the extensive research endeavor of exploring quantum states and establishing a structure-property relationship in correlated materials [10-12]. Due to the intimate coupling among charge, spin, orbital and lattice, modulations in quantum states can be very complicated, challenging the existing methodology for both probing and comprehending their nature [1,4]. In particular, modulations in crystals arise from not only periodicity but also discreteness in the arrangements of constituent electrons and ions. Lacking accurate description of the modulation would lead to an incomplete understanding, preventing us from delving the underlying physics.

Mathematically, collective phenomena of many quantum states or a structural modulation can be depicted by a complex order parameter, which is usually expressed as a wave function that can be expanded in the form of a discrete Fourier series [13-15]. In general, the phase and amplitude for each Fourier component are all constants regardless whether the wave periodicity is commensurate or incommensurate [13-16]. The simplest case of a wave with single wave-vector **q** is illustrated in Fig. 1(a) for a one-dimensional modulation. Increasing dimensions in the wave-vector space (multiple-**q**) only adds independent Fourier components, leaving the phase and amplitude of each **q**-vector constant [13]. Nevertheless, in reality, a long-range modulation can be easily disrupted by singularities in the material, which could come from defects in crystal lattice, like edge dislocation and antiphase boundary (APB) [17,18], and/or discontinuities in electronic structures, e.g., extra

charge localization at individual ions [12,19-21]. Consequently, the constant phase and amplitude in the modulation wave can be broken, which induces variations, such as topological phase defects and solitons [12,20-23]. A singularity in the phase of modulations, i.e., a phase shift, is presented in Fig. 1(b). Those singularities may vary the correlation length (e.g., forming domains depending on the dimensionality) and can substantially modify physical properties [24]. The distribution of phase singularities can be random or periodic in real-space as a result of competing energies in the system. In the case of periodically-distributed phase singularities, a new wave-vector **q** can be given for singularities in addition to the wave-vector **q** of the modulation. These two **q**-vectors are in principle independent, however, to date, only one experimental observation was reported for a case with two **q**-vectors along the same direction and the modulation amplitude remains unchanged [20]. All the above works suggest that modulations may exist with additional degrees of freedom in both phase and amplitude parameter spaces in a variety of materials. Understanding these modulations would advance our knowledge on the structural origin of properties and the modified phase and amplitude may assist the interpretation of the entanglement in quantum materials.

In this Letter, we present a study of an emergent modulation in a hole-doped CO system $LuFe_2O_{4+\delta}$ (δ is around 0.15) using advanced scanning transmission electron microscopy (STEM). The finding is schematically illustrated in Fig. 1(c), i.e., the phase and amplitude are characterized to be associated with a well-defined secondary wave, being a function of second-order modulation vector ($\mathbf{q_s}$) and position vector (**r**). Indeed, this can be considered as a universal expression of an order parameter, which might be applicable to diverse ordered systems. Insights from this work may also shed light on deciphering how the doped holes entangle with charge and lattice that determines many emergent quantum states in materials.

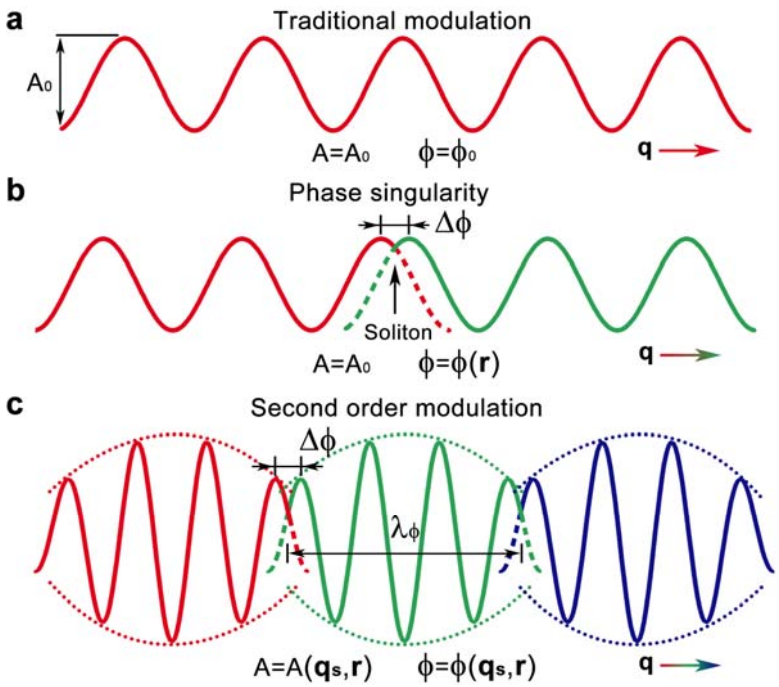

FIG. 1. Sketches of different types of modulation. (a) Traditional modulation (single wave-vector **q**). Both phase (ϕ_0) and amplitude (A_0) are constants. (b) A singularity in the modulation phase, i.e., a phase shift ($\Delta\phi$), generates phase variations with position vector (**r**). (c) Second order modulation. Phase and amplitude are modulated by a secondary wave, being a function of second-order modulation wave-vector ($\mathbf{q_s}$) and position vector (**r**).

$LuFe_2O_4$ is a model system with room-temperature CO. It has triangular bilayers of FeO_5 bipyramids sandwiched between Lu-O layers along **c**-direction (Fig. 2(a)) and space group $R\bar{3}m$ [25-27]. An equal amount of Fe^{2+} and Fe^{3+} ions on the triangular lattice forms the charge frustration due to energy degeneracy [28], depending on the excess of electron or hole on the third triangular corner (Fig. 2(a), lower panel). This arrangement makes its ground states highly susceptible to charge fluctuations, composition and temperature, leading to structural flexibility and chemical sensitivity [29-31]. Many interesting diffraction patterns have been observed and a series of intermediate states can be obtained upon doping [29-32], which therefore make it a very suitable platform for achieving and exploring emergent modulations.

Figure 2(b) shows an electron diffraction pattern (EDP) along [100] zone axis of the hole-doped $LuFe_2O_{4+\delta}$. Apart from fundamental spots, a constellation of satellite reflections that are absent in the stoichiometric sample (δ=0, Fig. S1) is observed, suggesting a modulated structure. Detailed inspections of EDP (Fig. 2(c)) reveal that sharp satellite reflections align well along $\mathbf{g_1}=[027]^*$ direction (we hereafter refer as primary modulation (PM) spots, indexed as $(hkl,m_1,0)$), which can be characterized by an incommensurate modulation wave-vector $\mathbf{q_p}$ ($\sim 0.135\mathbf{g_1}$). Importantly, it is noticed that each PM spot is accompanied by a second order modulation (SOM) spot (indexed as (hkl,m_1,m_2) with $m_1=m_2=\pm 1$) running along $\mathbf{g_2}=[01\bar{7}]^*$ direction, marked as $\mathbf{q_s}$ ($\sim 0.110\mathbf{g_2}$) in Fig. 2(c). This scenario manifests a marked difference from the traditional two-dimensional modulation [13,15,16], where two sets of first-order modulation spots appear both around fundamental spots.

To unravel this emergent modulation, quantitative analysis of the atomically-resolved high-angle annular dark-field (HAADF)-STEM image (Fig. 2(e)) was conducted using peak-pair algorithm (Supplemental Part 1) [33,34]. Periodic lattice displacement (PLD) maps of Lu along vertical [001] (Fig. 2(f)), and horizontal [120] directions (Fig. S2) were acquired. The most prominent feature is that the stripes of positive and negative displacement alternatively distribute along $[027]^*$ direction, yielding a periodicity of around 10 Å, consistent with PM spots ($\lambda=1/|\mathbf{q_p}|\approx 10.2$ Å). Displacement vectors in Fig. 2(g) follow a serpentine curve along $\mathbf{q_p}$ direction, which generates a sinusoidal PM wave as demonstrated in the displacement line profile (Fig. 2(h)). It is noteworthy that in PLD maps (Fig. 2(f), Fig. S2) positive and negative displacement stripes are not well-aligned but periodically glide along $(01\bar{7})$ plane, indicated by the white dash lines. Its periodicity is about 20 Å, being consistent with SOM spots ($\lambda_s=1/|\mathbf{q_s}|\approx 20.89$ Å). As revealed by the line trace (Fig. 2(h)), this glide is caused by the singularity in PM wave phase, i.e. a phase shift, $\Delta\phi=2\pi d/\lambda\approx 0.17\times 2\pi$. Periodic singularities generate a modulated phase along $\mathbf{q_s}$ direction, yielding a SOM. The same observation is reproduced by rotating the scanning direction 90 degrees during the

image acquisition (Fig. S3), thus ruling out the possible artifacts. Further inspections of PLD maps and line profiles reveal that the amplitude of PM also varies with position vector (**r**) and forms an oscillation, indicated by envelopes of lines in Fig. 2(h). The amplitude minima occur at the positions where phase singularity takes place. This situation is consistent with the previous theoretical prediction that the modulation amplitude collapses at phase deformations to prevent divergence of energy density [40,41].

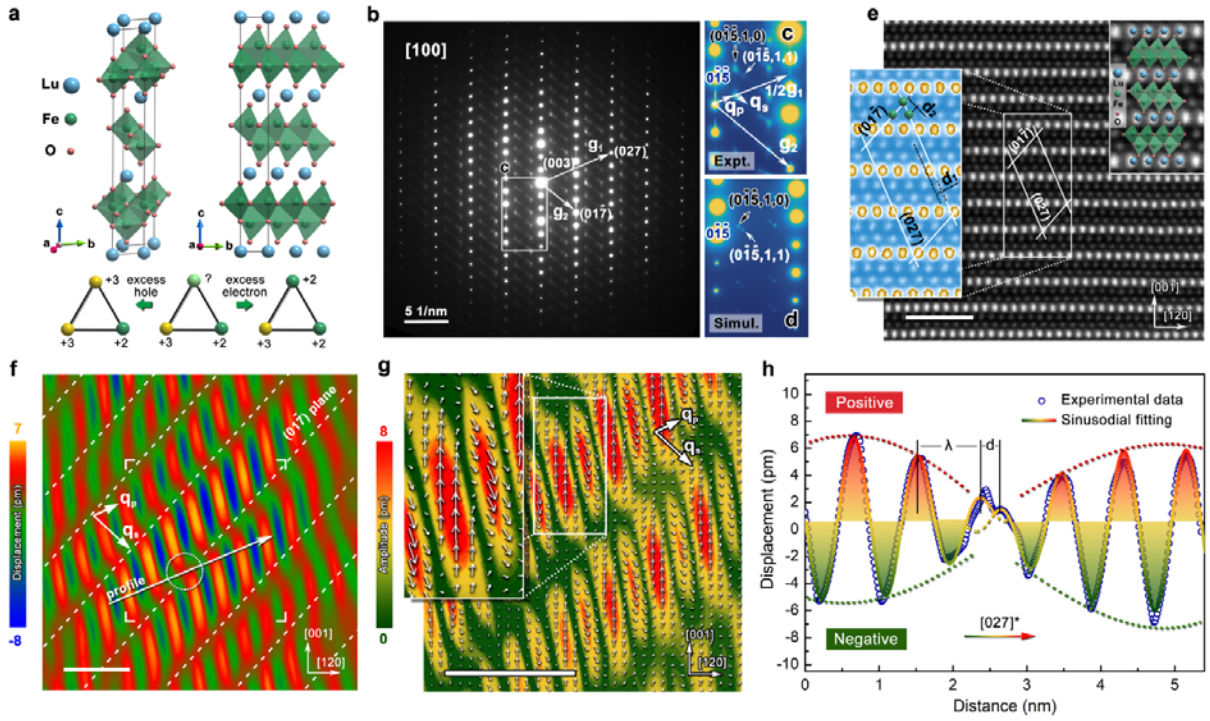

FIG. 2. Second order incommensurate modulation. (a) The left side of upper panel demonstrates the three-dimensional rhombohedral structure of $LuFe_2O_4$, and its projection along the **a**-axis is shown on the right side. Lower panel illustrates charge frustration. (b) [100] zone axis EDP with a series of satellite reflections. (c) Close-up of region marked in (b). Two vectors, $\mathbf{q_p}$ (~0.135$\mathbf{g_1}$) and $\mathbf{q_s}$ (~0.110$\mathbf{g_2}$), are assigned for PM and SOM spots, respectively. (d) Simulated EDP considering both PM and SOM (Eqn. (2)). The fourth (m_1) and fifth (m_2) index correspond to $\mathbf{q_p}$ and $\mathbf{q_s}$, respectively. (e) HAADF-STEM image along the **a**-axis. Spacings of the parallelogram correspond to real-space distances of $\mathbf{q_p}$ and $\mathbf{q_s}$. d_1 and d_2 are (027) and $(01\bar{7})$ planar distance, respectively. (f) PLD map

along the [001] direction. Periodic phase shift occurs at $(01\bar{7})$ planes, indicated by the broken white lines. (g) Displacement vector map of Lu extracted from delimiters-framed area in (f). A blow-up of the marked section is shown. Arrows follow displacement directions. Arrow length and color-coded background represent the amplitude. (h) Displacement line profile along $\mathbf{q_p}$ marked in (f), showing the phase shift ($\Delta\phi=2\pi d/\lambda$) and amplitude oscillation, outlined by envelopes of lines. All scale bars are 2 nm.

In general, PLDs can be depicted by a complex order parameter, which can be mathematically expanded in the form of discrete Fourier series with constant phase and amplitude for each component [13-16]. Traditionally, for a double-**q** case ($\mathbf{q_1}$, $\mathbf{q_2}$), the displacement (**u**) of atom-μ can be represented by,

$$\mathbf{u}(\mu,\mathbf{r}^{\mu}) = \mathbf{A}_1^{\mu}\sin\left[2\pi(\mathbf{q_1}\cdot\mathbf{r}^{\mu}+\phi_1^{\mu})\right] + \mathbf{A}_2^{\mu}\sin\left[2\pi(\mathbf{q}_2\cdot\mathbf{r}^{\mu}+\phi_2^{\mu})\right]. \quad (1)$$

$\mathbf{r}^{\mu} = \mathbf{T} + \mathbf{r}_{\mathbf{b}}^{\mu}$ is the position vector with the lattice vector (**T**) and the position of atom-μ in the basic structure ($\mathbf{r}_{\mathbf{b}}^{\mu}$). $\mathbf{A_1}$, $\mathbf{A_2}$ and ϕ_1, ϕ_2 are amplitudes and phases for $\mathbf{q_1}$ and $\mathbf{q_2}$, respectively, which are independent and constants. In our case, although there also exist two **q**-vectors ($\mathbf{q_p}$, $\mathbf{q_s}$), an attempt to describe the modulation using above formula leads to a failure (Supplemental Part 2 and Fig. S4). According to experimental observations, a new type of modulation wave is defined.

$$\mathbf{u}(\mu,\mathbf{r}^{\mu}) = \mathbf{A}_{\mathbf{p}}^{\mu}(\mathbf{q_s},\mathbf{r}^{\mu})\sin\left\{2\pi\left[\mathbf{q_p}\cdot\mathbf{r}^{\mu}+\phi_{\mathrm{p}}^{\mu}(\mathbf{q_s},\mathbf{r}^{\mu})\right]\right\}, \quad (2)$$

with $\mathbf{A}_{\mathbf{p}}^{\mu}(\mathbf{q_s},\mathbf{r}^{\mu}) = \mathbf{B}_{\mathbf{s}}^{\mu} + \mathbf{A}_{\mathbf{s}}^{\mu}\sin[2\pi(\mathbf{q_s}\cdot\mathbf{r}^{\mu}+\phi_{\mathrm{s}}^{\mu})]$ and $\phi_{\mathrm{p}}^{\mu}(\mathbf{q_s},\mathbf{r}^{\mu}) = 0.17\times Integer\,(\mathbf{q_s}\cdot\mathbf{r}^{\mu})$. $\mathbf{B}_{\mathbf{s}}^{\mu}$, $\mathbf{A}_{\mathbf{s}}^{\mu}$ and ϕ_{s}^{μ} are constants. Compared with Eqn. (1) that has Fourier terms for $\mathbf{q_1}$ and $\mathbf{q_2}$ separately, there exists only Fourier term for PM ($\mathbf{q_p}$). More importantly, phase and amplitude of PM are modulated by a SOM wave instead of being constants and become a function of SOM wave-vector ($\mathbf{q_s}$) and position vector (**r**). In this way, PM ($\mathbf{q_p}$) and SOM ($\mathbf{q_s}$) are intertwined, and their essential nature differs from the traditional two-dimensional modulation [13]. Based on Eqn. (2), systematical

simulations using Bloch-wave method can well reproduce experimental observations in both reciprocal- and real- space (Fig. 2(d), Fig. S4(d)).

Apart from this harmonious SOM, randomly-distributed nascent topological defects, like phase dislocations, were also observed (Fig. S5). Such phase defects have been previously reported in, for example, charge-ordered manganites [12,21,24], which could come from impurities, elastic strain and/or discontinuities in electronic structures [41,42]. Serving as pinning centers, they can break the long-range ordering of SOM, which accounts for the diffuse nature of SOM spots in our experiments.

As the PLDs are essentially generated by the modulation of charge density via charge-lattice coupling, this SOM has its origin in the abnormal charge distributions caused by doped holes. The hole doping nature was confirmed in Fig. S6 [43]. Charge modulation was further attested using atomically-resolved electron energy-loss spectroscopy (EELS). It is well-known that features of $L_{2,3}$ edges, including shape [47], position [48,49] and L_3/L_2 ratio [35,50], serve as fingerprints for the transition-metals' valency. Spectroscopic data of Fe-$L_{2,3}$ edges and HAADF-STEM image were simultaneously acquired pixel-by-pixel (Fig. 3(a), inset). The spectrum image clearly shows atomic Fe-sublattice, manifesting the high spatial resolution achieved to investigate individual Fe-columns. Fig. 3(a) demonstrates three post-processed Fe-$L_{2,3}$ edges from sites A-C. Since the higher energy of edge-onset and L_3/L_2 ratio for Fe correspond to higher oxidation states (below Fe^{3+}) [35,49,50], the valence increases monotonically from Site-C to Site-A. We then extracted all L_3/L_2 ratios, color-coded and overlaid on Fe-sublattice (Fig. 3(b)). Clear charge oscillations are visualized, which can be well fitted by a series of (027) and $(01\bar{7})$ planes with a periodic phase shift ($\Delta\phi$). The integration of L_3/L_2 ratios at each (027) plane along $\mathbf{q_p}$-direction (Fig. 3(c)), further confirms such a phase shift, yielding $\Delta\phi \approx 0.20 \times 2\pi$. This is consistent with structural modulation wave (Fig. 2(h)) and diffraction calculations (Fig. S4(d)). We note that measurements of L_3/L_2 ratios have rather large error bars, which may come from the well-documented effects, such as inelastic delocalization and

probe broadening [51-53]. Deviation from the model may be related to the small imperfection of the area and/or the random error in measurement. These observations manifest the quasiperiodic singularity in the phase of charge modulation, which accounts for the discontinuities of PLDs and can also be well described by the SOM defined in Eqn. (2).

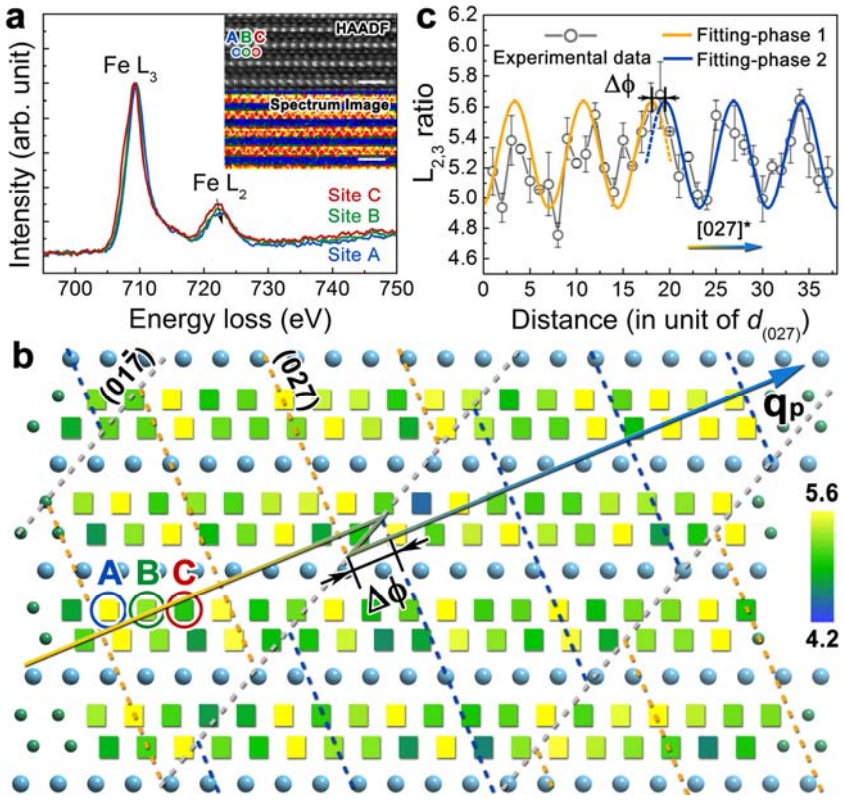

FIG. 3. EELS characterizations showing charge discontinuity. (a) EELS spectra at Site A-C extracted from the atomically-resolved spectrum image of Fe-$L_{2,3}$ edges in the inset. (b) Color-coded Fe-L_3/L_2 ratios extracted from each atomic column in spectrum image. Mesh spacings correspond to real-space distances of $\mathbf{q_p}$ and $\mathbf{q_s}$. (c) Integration of L_3/L_2 ratios at each (027) plane at the arrow position in (b). Experimental data can be fitted by two sinusoidal waves with a phase shift ($\Delta\phi$). Scale bars are 1 nm.

Previous studies on HTSCs suggested that local structural features and changes in carrier density for superconductivity depend on interstitial oxygens (O_i) [10]. Therefore, to unravel the origin of this charge-lattice SOM, the most stable O_i position in $LuFe_2O_{4+\delta}$ unit-cell was determined

by DFT calculations (Supplemental Part 3) [54]. Due to the **c**-axial layered structure, considering possible interstitial sites in one stacking block is sufficient (Fig. S7). Typical interstitial sites are labeled with A-E in **a**-**b** plane (Fig. 4(a), left panel) and each with different z-positions, indicated by vertical lines (right panel). For each site, ground state energies are calculated as a function of z-position and the potential-energy surface is obtained (Fig. 4(b)). To minimize the influence of O_i-O_i coupling, we take the lowest energy as reference and compare the relative total energy. It is found that Site-A is energetically favorable for all z-positions due to the largest void volume. Among all the A sites (different z-positions), one particular site denoted as Site-A_0 (z/c=0.7816) has the shortest Fe-O_i bond length and the lowest energy. Importantly, this site resides right at the junction of two edge-sharing planes of FeO_5 cages (Fig. 4(b), inset), which is the intersection of (027) and $(01\bar{7})$ planes.

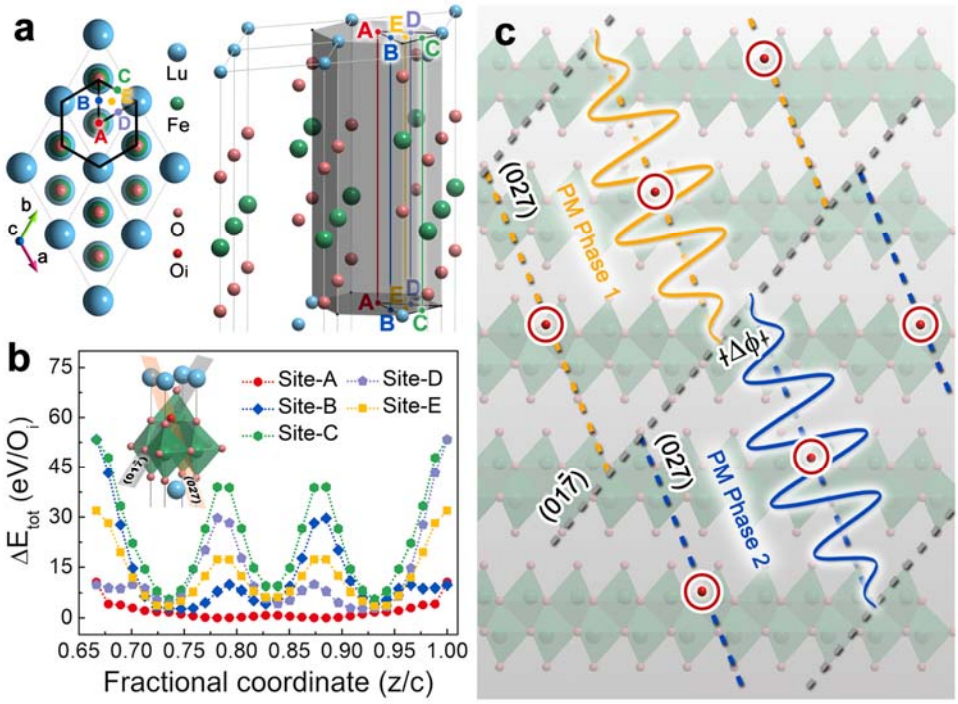

FIG. 4. DFT calculations on the origin of SOM. (a) Five isolated interstitial sites considered in calculations, indexed from A to E in **a**-**b** plane (left panel). Each site consists of a series of z-positions, indicated by vertical lines (right panel). (b) The relative total energies (eV/O_i) as a function of the fractional coordinate. Polyhedron exhibits the lowest-energy site (Site-A_0) with

z/c=0.7816. (c) A schematic illustrating the charge-lattice SOM. O_i resides at the lowest-energy site based on calculations. Lutetium is omitted for clarity. The discontinuity of displacement magnitude-damping curves (blue and yellow) induces the phase glide ($\Delta\phi$).

Combing the calculations with experiments, a possible mechanism for SOM is proposed (Fig. 4(c)). Based on PLD and charge mapping results, a mesh consisting of a series of (027) and $(01\bar{7})$ planes was drawn to translate (027) planes passing through the lowest-energy O_i. Since ionic displacements are essentially caused by O_i, their magnitude reaches a maximum at O_i-site and damps down with the increase in distance. Consequently, it yields periodic displacement damping curves (yellow for Phase 1, blue for Phase 2) along the (027) plane. As two damping curves cannot merge at the $(01\bar{7})$ plane, a glide operation forms that generates phase discontinuities and amplitude oscillations in the PM. Meanwhile, local electronic structure and charge density are also modified by O_i, as revealed by EELS results. In this picture, interstitial oxygens serving as solitons bring singularities in both lattice and charge modulations, which is analogous to the case in hole-doped cuprates [20]. Periodic singularities introduce a secondary order into PM phase and amplitude along $\mathbf{q_s}$ direction. Meanwhile, a new periodicity for $(01\bar{7})$ planes related to SOM spots forms. Eventually, PM phase and amplitude are modulated by a SOM wave and dependent on the SOM wave-vector $\mathbf{q_s}$ and position vector $\mathbf{r}$, leading to intertwined PM and SOM, as defined in Eqn. (2).

The distribution of singularities in modulation can be random [12,21] or periodic in real-space (this study) as a result of competing energies in the system. On the basis of our experimental observations, DFT calculations, and simulations, we propose a new paradigm of modulating phase and amplitude parameter spaces by a second-order wave ($\mathbf{q_s}$). As illustrated in the modulation formula (Eqn. (2)), a $\mathbf{q}$-vector (e.g., $\mathbf{q_2}=\mathbf{q_s}$) is introduced into phase and amplitude field ($\mathbf{u}=\mathbf{u_1}[\mathbf{q_1}, A_1(\boldsymbol{q_2}), \phi_1(\boldsymbol{q_2})]$) rather than as an independent Fourier component ($\mathbf{u}=\mathbf{u_1}(\mathbf{q_1})+\boldsymbol{u_2}(\boldsymbol{q_2})$) [13].

This concept is readily generalizable to multiple-**q** cases. Phase and amplitude for all Fourier components can be independently modulated by a second-order wave ($\mathbf{q_s}^j$), i.e. $\mathbf{u} = \sum_{i,j} \mathbf{u}_i[\mathbf{q}_i, \mathrm{A}_i(\mathbf{q_s}^j), \phi_i(\mathbf{q_s}^j)]$. Based on this framework, additional degrees of freedom are essentially added in both phase and amplitude parameter spaces. This formulism provides a more accurate and universal depiction of the order parameter and can be widely applicable to numerous ordered systems, as singularities are ubiquitous [12,21-24,42].

Conclusions

In summary, by purposely introducing excess holes in a prototype charge-ordered system $LuFe_2O_{4+\delta}$, we observed a new type of modulation with its phase and amplitude modulated by a second order modulation wave using state-of-the-art electron microscopy. By directly measuring lattice and charge components at atomic scale, quasiperiodic singularities are found in both periodic lattice displacements and charge modulation. We show that due to the interplay between interstitial oxygens, lattice locking, and charge frustration, the phase and amplitude of primary modulation can be tuned by quasiperiodic singularities, engendering a second order modulation wave. Through introducing a **q**-vector into amplitude and phase parameter spaces, new modulation formulism is developed. Our study illustrates a new approach to manipulate singularity in modulation waves via targeted hole doping to understand intriguing behavior of quantum materials.

Acknowledgments

The electronic microscopy study was carried out at Brookhaven National Laboratory and supported by the U.S. DOE Basic Energy Sciences, Materials Sciences and Engineering Division under Contract No. DESC0012704. J. Z., S. D., and S. C. would like to acknowledge the financial support by Chinese National Natural Science Foundation under Project No. 51390471 and the National 973 Project of China (Project No. 2015CB654902) as well as the support of S. D. for

studying abroad from China Scholarship Council. This work made use of the resources of the National Center for Electron Microscopy in Beijing. The theoretic work was done at Xiamen University. The research at Fudan University was supported National Key Research and Development Program of China (Grants No. 2016YFA0300702); National Natural Science Foundation of China (Grant No. 11504053); Program of Shanghai Academic Research Leader (Grant No. 17XD1400400); National Key Research and Development Program of China (Grants No. 2016YFA0300702). We thank Wei Wang for very helpful discussion and help on the quantitative analysis of electron microscopy images.

†Corresponding author: jzhu@mail.tsinghua.edu.cn

*Corresponding author: zhu@bnl.gov

^ Visiting student at Brookhaven National Laboratory

Reference

[1] E. Dagotto, Science **309**, 257 (2005).

[2] H. Alloul, J. Bobroff, M. Gabay, and P. J. Hirschfeld, Rev. Mod. Phys. **81**, 45 (2009).

[3] G. Ghiringhelli *et al.*, Science, **337**, 821 (2012).

[4] J. Chang *et al.*, Nat. Phys. **8**, 871 (2012).

[5] X.-L. Qi and S.-C. Zhang, Rev. Mod. Phys. **83**, 1057 (2011).

[6] P. W. Anderson, *Basic Notions Of Condensed Matter Physics* (CRC Press, Taylor & Francis Group, 1997).

[7] T. Ritschel, J. Trinckauf, K. Koepernik, B. Büchner, M. v. Zimmermann, H. Berger, Y. I. Joe, P. Abbamonte, and J. Geck, Nat. Phys. **11**, 328 (2015).

[8] H. v. Löhneysen, A. Rosch, M. Vojta, and P. Wölfle, Rev. Mod. Phys. **79**, 1015 (2007).

[9] U. Staub, G. I. Meijer, F. Fauth, R. Allenspach, J. G. Bednorz, J. Karpinski, S. M. Kazakov, L. Paolasini, and F. d'Acapito, Phys. Rev. Lett. **88**, 126402 (2002).

[10] Y. Gao, P. Lee, P. Coppens, M. A. Subramanian, and A. W. Sleight, Science **241**, 954 (1988).

[11] R. Comin *et al.*, Nat. Mater. **14**, 796 (2015).

[12] B. H. Savitzky, I. El Baggari, A. S. Admasu, J. Kim, S. W. Cheong, R. Hovden, and L. F. Kourkoutis, Nat. Commun. **8**, 1883 (2017).

[13] A. J. C. Wilson and E. Prince, *International tables for crystallography* (Kluwer academic publishers, 1999), 2nd. Ed., Vol. C Mathematical, physical and chemical tables, p. 899-907.

[14] P. M. de Wolf, Acta Crystallogr., Sect. A: Cryst. Phys., Diffr., Theor. Gen. Crystallogr. A **33**, 493 (1977).

[15] J. M. Perez-Mato, G. Madariaga, F. J. Zuñiga, and A. Garcia Arribas, Acta Crystallogr., Sect. A **43**, 216 (1987).

[16] A. Yamamoto, Acta Crystallogr., Sect. A: Cryst. Phys., Diffr., Theor. Gen. Crystallogr. **38**, 87 (1982).

[17] D. T. Margulies, F. T. Parker, M. L. Rudee, F. E. Spada, J. N. Chapman, P. R. Aitchison, and A. E. Berkowitz, Phys. Rev. Lett. **79**, 5162 (1997).

[18] T. Hibma, F. C. Voogt, L. Niesen, P. A. A. van der Heijden, W. J. M. de Jonge, J. J. T. M. Donkers, and P. J. van der Zaag, J. Appl. Phys. **85**, 5291 (1999).

[19] W. L. McMillan, Phys. Rev. B **14**, 1496 (1976).

[20] C. Guo, H. F. Tian, H. X. Yang, B. Zhang, K. Sun, X. Sun, Y. Y. Peng, X. J. Zhou, and J. Q. Li, Phys. Rev. Mater. **1**, 064802 (2017).

[21] I. El Baggari, B. H. Savitzky, A. S. Admasu, J. Kim, S. W. Cheong, R. Hovden, and L. F. Kourkoutis, Proc. Natl. Acad. Sci. U. S. A. **115**, 1445 (2018).

[22] W. S. Lee *et al.*, Nat. Commun. **3**, 838 (2012).

[23] P. Zhu *et al.*, Appl. Phys. Lett. **103**, 071914 (2013).

[24] J. Tao *et al.*, Sci. Rep. **6**, 37624 (2016).

[25] M. Isobe, N. Kimizuka, J. Iida, and S. Takekawa, Acta Crystallogr. Sect. C: Cryst. Struct. Commun. C **46**, 1917 (1990).

[26] Y. Zhang, H. X. Yang, Y. Q. Guo, C. Ma, H. F. Tian, J. L. Luo, and J. Q. Li, Phys. Rev. B **76**, 184105 (2007).

[27] N. Ikeda *et al.*, Nature **436**, 1136 (2005).

[28] Y. Yamada, K. Kitsuda, S. Nohdo, and N. Ikeda, Phys. Rev. B **62**, 12167 (2000).

[29] M. Hervieu, A. Guesdon, J. Bourgeois, E. Elkaim, M. Poienar, F. Damay, J. Rouquette, A. Maignan, and C. Martin, Nat. Mater. **13**, 74 (2014).

[30] S. Cao, J. Li, Z. Wang, H. Tian, Y. Qin, L. Zeng, C. Ma, H. Yang, and J. Li, Sci. Rep. **2**, 330 (2012).

[31] Y. Zhang, H. X. Yang, C. Ma, H. F. Tian, and J. Q. Li, Phys. Rev. Lett. **98**, 247602 (2007).

[32] J. de Groot, T. Mueller, R. A. Rosenberg, D. J. Keavney, Z. Islam, J.-W. Kim, and M. Angst, Phys. Rev. Lett. **108**, 187601 (2012).

[33] P. Galindo, J. Pizarro, S. Molina, and K. Ishizuka, Microsc. Anal.-UK **130**, 23 (2009).

[34] See Supplemental Material for details of experiments and quantitative analysis, which include Refs. [35-39].

[35] P. A. van Aken and B. Liebscher, Phys. Chem. Miner. **29**, 188 (2002).

[36] J. Mayer, L. Giannuzzi, T. Kamino, and Joseph Michael, MRS Bull. **32**, 400 (2007).

[37] K. Thompson, B. Gorman, D. J. Larson, B. van Leer and L. Hong, Microsc. Microanal. **12** (S02) 1736 (2006).

[38] Z. Huang, J. Microsc. **215**, 219 (2004).

[39] P. L. Galindo, S. Kret, A. M. Sanchez, J. Y. Laval, A. Yanez, J. Pizarro, E. Guerrero, T. Ben, and S. I. Molina, Ultramicroscopy **107**, 1186 (2007).

[40] D. Feinberg and J. Friedel, J. Phys. France **49**, 485 (1988).

[41] S. N. Coppersmith and A. J. Millis, Phys. Rev. B **44**, 7799 (1991).

[42] J. Tao, K. Sun, J. M. Tranquada, and Y. Zhu, Phys. Rev. B **95**, 235113 (2017).

[43] See Supplemental Material for EELS spectra analysis, which includes Refs. [44-46].

[44] R. F. Egerton, *Electron energy-loss spectroscopy in the electron microscope*, (Springer

Science+Business Media, LLC 2011), 3rd.

[45] L. A. Grunes, R. D. Leapman, C. N. Wilker, R. Hoffmann, and A. B. Kunz, Phys. Rev. B **25**, 7157 (1982).

[46] J. A. Mundy, Q. Mao, C. M. Brooks, D. G. Schlom, and D. A. Muller, Appl. Phys. Lett. **101**, 042907 (2012).

[47] J. H. Paterson and O. L. Krivanek, Ultramicroscopy **32**, 319 (1990).

[48] M. T. Otten, B. Miner, J. H. Rask, and P. R. Buseck, Ultramicroscopy **18**, 285 (1985).

[49] H. Tan, J. Verbeeck, A. Abakumov, and G. Van Tendeloo, Ultramicroscopy **116**, 24 (2012).

[50] S. Deng, S. Cheng, C. Xu, B. Ge, X. Sun, R. Yu, W. Duan, and J. Zhu, ACS Appl. Mater. Interfaces **9**, 27322 (2017).

[51] L. J. Allen, S. D. Findlay, M. P. Oxley, C. Witte, and N. J. Zaluzec, Ultramicroscopy **106**, 1001 (2006).

[52] H. Tan, S. Turner, E. Yücelen, J. Verbeeck, and G. Van Tendeloo, Phys. Rev. Lett. **107**, 107602 (2011).

[53] C. Mitterbauer, G. Kothleitner, W. Grogger, H. Zandbergen, B. Freitag, P. Tiemeijer, and F. Hofer, Ultramicroscopy **96**, 469 (2003).

[54] See Supplemental Material for details of DFT calculations, which include Refs. [55-57].

[55] P. Giannozzi, *et al.*, J. Phys. Condens. Matter. **21**, 395502 (2009).

[56] J. P. Perdew, K. Burke, and M. Ernzerhof, Phys. Rev. Lett. **77**, 3865 (1996).

[57] K. F. Garrity, J. W. Bennett, K. M. Rabe, and D. Vanderbilt, Comput. Mater. Sci. **81**, 446 (2014).